International Journal of Adhesion and Adhesives 82 (2018) 126–138

Contents lists available at ScienceDirect

International Journal of Adhesion and Adhesives

journal homepage: www.elsevier.com/locate/ijadhadh

Failure behaviour of silicone adhesive in bonded connections with simple geometry

Yves Staudt[a], Christoph Odenbreit[a,*], Jens Schneider[b]

[a] University of Luxembourg, L-1359 Luxembourg, Luxembourg
[b] Technische Universität Darmstadt, D-64295 Darmstadt, Germany

ARTICLE INFO

Keywords:
A. Silicones
C. Finite element stress analysis
D. Mechanical properties of adhesives
Failure criterion

ABSTRACT

In façade structures, adhesively bonded connections between glass panels and metallic substructures represent an attractive alternative to mechanical fixation devices. Apart from positive aspects regarding the construction's energy efficiency and aesthetics, the uniform load transfer reduces stress concentrations in the adherends, which is beneficial especially regarding brittle materials like glass. Structural silicone sealants are generally used for these kind of applications due to their excellent adhesion on glass and their exceptional resistance against environmental influences and ageing. For the verification of the bonded connection, non-linear numerical simulations, such as the Finite Element Method, are increasingly used. The resulting three-dimensional stress states need to be assessed with the help of an appropriate failure criterion. In this paper, an overview is given on available failure criteria for rubber-like materials. The applicability of these criteria on the silicone sealant is verified regarding three characteristic stress states: uniaxial tension, shear and compression. The proposed engineering failure criterion is the true strain magnitude, which is valid for bonded connections in form of linear beads for cohesive failure of the adhesive. For Dow Corning® 993 structural silicone sealant, the strain magnitude, evaluated using true strains, at failure could be determined as 1.6.

1. Introduction

1.1. Structural sealant glazing systems

In façade applications, the usage of glass has constantly increased over the last decades. Glass is chosen in an attempt to create on the one hand an architectural attractive façade and on the other hand a highly transparent building skin, allowing for the usage of natural illumination [1]. Regarding the brittle material behaviour of glass, the inevitably question of its connection to the mostly metallic substructure becomes crucial. Different techniques, such as mechanical and adhesive connections, can be envisaged [2].

In the field of mechanical connections, glass can either be linearly supported or point-wise by bolted connections. The use of linear connections reduces the transparency of the façade and creates to a certain extend thermal bridges, because parts of the mechanical connection are in contact with the external surface of the building skin [3]. Bolted connections however significantly weaken the glass pane as boreholes have to be drilled into the glass. The related manufacturing process can generate scratches and flaws, which reduce the strength of glass. Furthermore, high stresses are generated in the glass pane due to the small area of load transfer between the bolt and the borehole [2].

In addition to the above mentioned mechanical connection possibilities, glass can also be adhesively bonded to the building's substructure. Although polyurethanes, which are used in automotive applications for steel to glass bonded connections, have higher strength and stiffness [4], only the usage of soft structural silicone sealants is covered by the European Technical Application Guideline (ETAG 002) [5] for façade applications. For adhesively bonded connections, both linear and point applications of the sealant can be found. Adhesively bonded connections with silicones in curtain wall façades were initially developed in the United States in the 1960s for two-side supported glass panes with the two other sides conventionally glazed (see Fig. 1) and later in application with all four edges adhesively bonded [6]. To increase the transparency of the façade, while avoiding the inconveniences of drilled-through bolts, adhesively bonded point-fixings are subject to research activities [7].

The main advantage of bonded connections with a soft adhesive like silicone, especially in linear applications, is the distributed load transfer due to the large bonding area. Moreover, differences in the deformation of the adherends due to structural movements or differential thermal expansions are compensated, thus reducing stress concentrations in the

* Corresponding author.
E-mail address: christoph.odenbreit@uni.lu (C. Odenbreit).

https://doi.org/10.1016/j.ijadhadh.2017.12.015
Accepted 14 December 2017
Available online 26 December 2017

Fig. 1. Example of a two-side supported structural glazing system: Kastor tower in Frankfurt/Main (Germany) [8].

substrates. Finally, silicone sealants can absorb a significant amount of energy, which is beneficial for their use in regions of high wind or seismic loading. Apart from an architectural attractive smooth building skin, the energy efficiency of the building is increased, as no mechanical retaining devices are penetrating the façade [3,6].

Silicone was developed in the early 20th century by the chemist Kipping [3]. After the curing of the sealant, silicone is an elastomer composed of cross-linked polymer chains. The molecular backbone of the polymer shows the particularity of having an organic structure with the inorganic components silicon and oxygen, instead of carbon. Furthermore, the low reactivity and the hydrophobic nature of silicone explains the outstanding resistance against ageing, UV and weather impact [3]. In addition, silicones show excellent adhesion properties on many materials, especially on glass [9]. In [10], the material properties of filled and unfilled silicones were investigated. Only a small quasi linear increase of the stiffness of the stress-strain curve was observed for temperatures within the range of civil engineering applications (− 20°C to 80°C).

The European Technical Application Guideline (ETAG 002) [5] and the equivalent guideline in the United States, ASTM C1401 [11] propose a design method for Structural Sealant Glazing Systems. Both design methods base on a linear analysis and assume a uniform load distribution inside the adhesive. The acting surface loads on the glass (e.g. wind loads) are distributed using trapezoidal load distribution areas. Due to the lack of an in-depth mechanical analysis of the material behaviour of the silicone, high design factors and restrictions in use are defined. Apart from these guidelines, no reliable analytical methods are available to analyse the complex stress states, especially when complex adhesive geometries are considered [4].

The material behaviour of silicones can be described assuming a non-linear elastic, or hyperelastic material law, when viscous effects are neglected [2]. As the bulk modulus of silicone is much higher than the shear modulus, it is often assumed as incompressible [4,12]. Due to the limitations of analytical approaches, adhesively bonded connections are often analysed using the Finite Element Method. There are a number of commercially available Finite Element software codes, in which hyperelastic material laws are implemented. An overview about hyperelastic material laws can be found in [2]. The result of a Finite Element Analysis is a three dimensional strain and stress state. The key task of the structural engineer is to assess this complex stress state. For this assessment, mathematical functions are generally used to transform the complex stress state into a scalar value, which can be compared to the results of simple material tests, like the uniaxial tension test. For silicone sealants, investigations on a damage initiation criterion have been performed in [13] and the strain energy density has been identified as a potential failure criterion. In this paper, additional investigations are presented on this subject.

1.2. Objectives and methodology

The objective of the current research project is to identify a suitable failure criterion for silicone joints in form of a linear bead with simple geometry, in which a deviatoric stress state is dominant. In order to identify a suitable failure criterion, experimental investigations on bulk material were conducted, focussing on the following characteristic stress states: (i) uniaxial tension, (ii) simple shear and (iii) compression.

For testing silicone sealants in shear, the European standard test specimen is foreseen by the ETAG 002 [5] as a linear silicone bead between two substrates. This kind of single lap shear joint however shows a stress singularity, the so-called two material wedge, at the corner edge of the interface. Therefore, when analysing this specimen in a Finite Element Analysis, the stresses and strains become dependent on the chosen discretisation of the sealant and thus to a certain extend arbitrary [14,15]. Since the mechanical behaviour of bulk material is investigated, a circular specimen has been chosen to avoid the stress singularities at the two material wedge.

In the following investigations, Dow Corning® 993, a two-component neutral curing structural silicone sealant [16] was studied. The subsequent experimental investigations are part of a PhD research project [17] at the University of Luxembourg in collaboration with TU Darmstadt, Germany.

2. Failure criteria for rubber-like materials

For the verification of a sufficient load-bearing capacity of a structure, an acting stress state is compared with an allowable upper limit. Especially for silicone sealants with their pronounced non-linear material behaviour, the acting stress state is often determined in a non-linear Finite Element Analysis using commercial Finite Element software codes. The result of these simulations are stress and strain tensors, which can be described in their diagonalised form by the three principal stresses and strains. For simplicity reasons, the upper limit is often defined using the tensile strength, measured in uniaxial tensile tests of dog-bone specimens. The challenge consists in the comparison and judgement of both stress states. An alternative for this assessment is the component test in 1:1 scale, which is however time consuming and expensive. Therefore, a criteria is required, which allows to transform the complex stress state in a value that can be compared with the results of the material strength determined in a one-dimensional test, like the uniaxial tensile test.

2.1. Three concepts to assess the complex stress state

In principle, the assessment of a complex stress state can be performed by following three different concepts [18] (Fig. 2). In a classic method, a perfect material without flaws and defects is assumed and the stress state is evaluated based on a fracture criteria, which is a

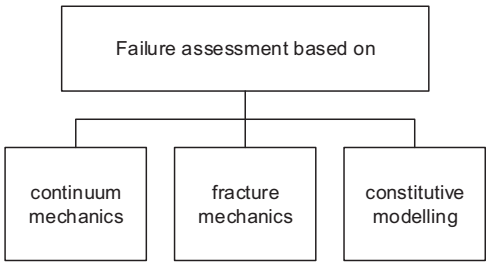

Fig. 2. Overview of concepts to assess failure.

mathematical function, working with mechanical quantities from a continuum mechanics approach. A second method is based on the assumption of pre-cracked specimens and adopts concepts from fracture mechanics to describe failure. Finally, promoted by the development of the Finite Element Method and the availability of ever more powerful hardware, the failure process can be included into the constitutive modelling of the material.

In the following investigations, only simple engineering failure criteria on (a) defect-free rubber-like bulk material are investigated for (b) the case of a static loading. For the failure criteria, a differentiation is generally made between stress-, strain- and energy-based functions. Stress based criteria are considered since they take into account the hydrostatic stress state, whereas strain based criteria are based on displacements, which can be directly compared with measured values.

2.2. Stress-based criteria

The principal stress hypothesis has been introduced by Rankine, Lamé and Navier and is often adopted as a failure criterion for brittle materials [19]. Failure occurs if either the maximum principal stress exceeds the tensile strength, or if the minimum principal stress is smaller than the compression strength.

$$\sigma_1 = \sigma_t \vee \sigma_3 = \sigma_c \tag{1}$$

In Eq. (1), σ_1 is the maximum principal stress, σ_t the tensile strength, σ_3 the minimum principal stress and σ_c the compression strength.

Failure of quasi-incompressible rubber-like material under triaxial stresses is often associated with internal growth of voids or cavities, the so-called cavitation. On a macroscopic scale, the failure initiation by void nucleation can be identified as a significant change of slope in the stress-strain diagram of a specimen [20]. Cavitation occurs for highly triaxial stress states, for which significant values of positive (tensile) hydrostatic stresses are obtained. These kind of stress states can be found for so-called pancake specimens under tensile loads. A pancake specimen consists of two butt bonded cylinders or a cylinder bonded on a flat surface with an adhesive thickness, which is small compared to the diameter of the cylinder [7]. In [20], pancake tests on rubber with different values of adhesive thickness have been performed. The fracture pattern of thin adhesive layers clearly exhibited small bubbles originating from cavitation prior to complete failure of the specimen. In addition, a clear change of slope was observed in the recorded force-deformation curves. For thick layers however, neither changes of slope in the recorded diagrams nor small bubbles were observed. The failure process of these specimens was not controlled by cavitation, but by crack initiation and crack propagation. The threshold value for void nucleation is given in Eq. (2) [20].

$$p = -1/3 I_\sigma < 5/6 E \tag{2}$$

In Eq. (2), p is the hydrostatic pressure, I_σ the first invariant of the Cauchy stress tensor and E Young's modulus of the considered sealant at small strains. The critical value 5/6 E has been analytically derived in [20] assuming a Neo-Hookean material law and experimentally validated on butt bonded cylinders under tensile loads.

The von Mises criterion was originally developed as a yield criterion for ductile materials, but since it is implemented in many commercial Finite Element software codes, it is also used to assess complex stress states within polymers. The von Mises yield criterion does not take into account a hydrostatic stress state [19]. The failure of rubber-like material however is dependent on the triaxiality of the stress state [20].

$$\sigma_{vM} = \sqrt{3 II_s} \tag{3}$$

In Eq. (3), σ_{vM} is the equivalent stress according von Mises, II_s the second invariant of the deviatoric stress tensor **s**, which is defined as: $\mathbf{s} = \boldsymbol{\sigma} - p\,\mathbf{I}$, where p is the hydrostatic pressure and **I** the unit tensor.

2.3. Strain-based criteria

The maximum principal strain hypothesis was introduced by Saint-Venant and Bach [19].

$$\varepsilon_1 = \varepsilon_t \tag{4}$$

In equation 4, ε_1 is the first principal strain and ε_t the ultimate strain. Amongst others, the maximum principal strain is widely used in fatigue life analysis of rubber [21].

The *strain magnitude* is also used to assess the stress state of rubber-like materials. The *strain magnitude* can be seen as a measure for the stretch of the molecular chains [22]. It is used with true strains, since rubber-like materials usually allows for large deformations.

$$\varepsilon_M = \sqrt{\varepsilon_1^2 + \varepsilon_2^2 + \varepsilon_3^2} \tag{5}$$

In equation 5, ε_M is the strain magnitude and ε_i ($i = 1..3$) are the true principal strains.

2.4. Energy-based criteria

Apart from the maximum principal strain, the *strain energy density* is often used for the fatigue life prediction of rubber-like material [21]. According to [22], the rupture of an elastomer occurs, when the binding energy between molecules is surmounted. This binding energy corresponds to the strain energy density, which is equivalent to the area under the stress-strain curve.

$$W = \int \sigma_{ij} d\varepsilon_{ij} \tag{6}$$

In Eq. (6), σ_{ij} are the components of the Cauchy stress tensor and ε_{ij} the components of the true strain tensor.

3. Numerical simulation of the structural silicone sealant

As already mentioned before, silicone sealants exhibit a highly non-linear material behaviour. Apart from time dependent phenomena like creep or relaxation, which have been considered in detail in [2], the material properties are to a certain extend depending on the applied strain rate, as investigated in [12]. Additionally, especially rubber-like materials exhibit the so-called stress-softening or Mullins effect [23]. The Mullins effect is a change of the mechanical properties after the first stretching of the material. The unloading path is softer than the initial loading path. If the material is extended again, the recorded stiffness is either coincident with the unloading path (ideal Mullins effect), or between the unloading and reloading path. Most of the softening appears after the first loading, for the following cycles, a stable response is obtained, when fatigue is disregarded. For extensions of the material beyond the maximum stretch ever applied before, the material response corresponds to the initial or virgin stress-strain path. The stress-softening effect was investigated for silicones in [12,23].

In the following investigations, the two component room temperature vulcanising Dow Corning® 993 [16] structural silicone sealant is numerically simulated for a constant strain rate of a quasi-static loading and for the initial, virgin material behaviour. As aforementioned, the silicone adhesive will be considered as incompressible, as its bulk

modulus is much higher than the shear modulus [2]. Moreover, ultrasonic measurements showed that the Poisson ratio is close to 0.5 [24]. In order to avoid cavitation phenomena, only linear beads of silicone adhesive with simple geometry are considered, in which the hydrostatic stress state is less dominant.

The numerical reproduction of rubber-like materials is often performed using hyperelastic material laws. The hyperelastic material laws are generally based on a functional expression using the invariants of the Cauchy-Green strain tensor. Amongst the phenomenological models, Neo-Hooke and Yeoh are depending on the first invariant only, whereas Mooney-Rivlin also uses the second. An overview of hyperelastic material laws for rubber is given in [2].

As investigated in [12], only the response function was able to represent the stiffness at the origin of the stress-strain curve of the investigated shear specimens with the considered Dow Corning® 993 adhesive. The response function, or Marlow hyperelastic material law [25], is not based on a functional expression for the strain energy density, but the strain energy density is supposed to depend only on the first invariant of the Cauchy-Green tensor. Therefore, for a given deformation state, an equivalent uniaxial stretch can be determined, which leads to the same value for the first invariant of the Cauchy-Green tensor as for the considered deformation state. With this equivalent uniaxial stretch, the strain energy density can be determined by a numerical integration of the experimental stress-strain curve up to the mentioned equivalent uniaxial stretch [25]. For Dow Corning® 993 silicone, the stress-strain curve in uniaxial tension from [12] (shown in Fig. 7) is used as input data for the Marlow hyperelastic material law.

4. Uniaxial tensile test

4.1. Specimen

For the uniaxial tensile tests, dumbbell or dog-bone shaped specimens according to ASTM D412 [26] were used. The geometry of the specimen is given in Fig. 3 and a picture is shown in Fig. 4.

In a first step, a sheet of silicone with a nominal thickness of 2 mm was poured on a polyethylene foil. After a week of curing time under controlled conditions at the manufacturer, dumbbell shaped specimens were punched out of the silicone sheet using appropriated punching tools. In the presented investigations, a total number of five specimens has been tested.

4.2. Test setup and measurement equipment

A Zwick testing machine with electronic drive having a capacity of 50 kN was used. The testing machine is shown in Fig. 5. The laboratory is air-conditioned to 23°C and 50% relative humidity.

As very low forces were expected due to the small cross-sectional area of the dumbbell-specimens and the relative low strength of silicone sealants compared to other engineering materials like steel or glass, an external 500 N load cell was used in addition to the 50 kN load cell of the testing machine to guarantee accurate measurement of the applied forces. The strains were measured locally on the surface of the specimens using video-extensometry. For this, circular thin red marks were poured on the silicone sealant to record the deformations on the narrow

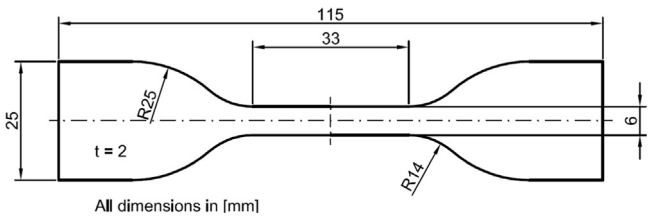

Fig. 3. Dimensions of the tensile test specimen according to ASTM D412 [26].

Fig. 4. Picture of the tensile test specimens according to ASTM D412 [26].

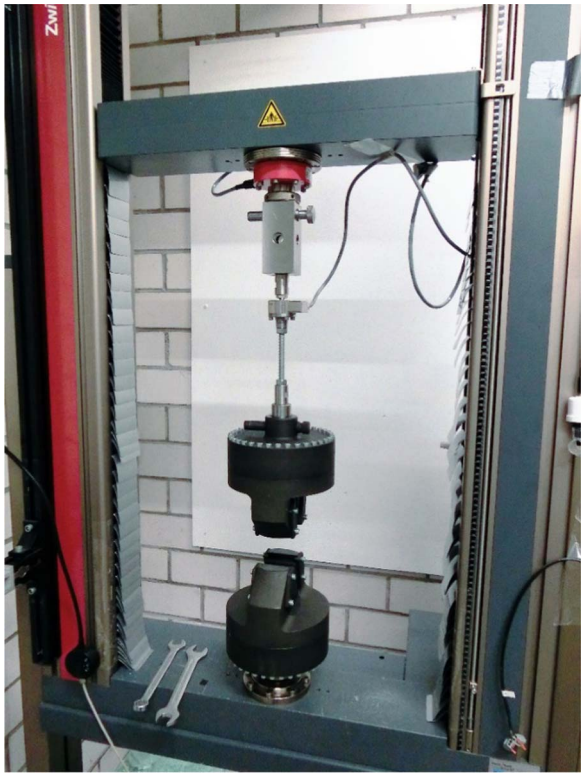

Fig. 5. 50 kN Zwick tensile testing machine at ISM + D, TU Darmstadt.

part of the specimens, see Fig. 4. One-component neutral curing red silicone sealant was used for this purpose, as no other suitable material could adhere on the sealant. The red marks had a diameter of 3 mm and a thickness of less than 0.5 mm. Considering the small dimensions of the marks and the low stiffness of silicone sealants compared to structural sealants, their influence on the overall behaviour was judged as negligible. A MATLAB® based software was used to analyse the video frames recorded during the test. The algorithm is presented in [27]. At each time step, which was synchronised with the signals of the load cell, the red surfaces were detected and the centre of gravity was determined for each mark. The evaluation bases on the principle, which is given in Fig. 6 and Eq. (7).

$$\varepsilon_{e,l,i} = \Delta l / l_0 = (l - l_0)/l_0 = (y_{i,2} - y_{i,1})/(y_{0,2} - y_{0,1}) - 1 \quad (7)$$

In Eq. (7), $\varepsilon_{e,l,i}$ is the longitudinal engineering strain at the time step i, l_0 the distance between the two red marks in the reference configuration, l the distance between the two red marks for the deformed shape and $y_{i,j}$ the ordinate of the red point's (j) centre of gravity at time step i.

The loading rate was set to 6 mm/min. The specimens' dimensions have been measured prior to each test.

4.3. Test results

The test results in terms of engineering stress-strain curves are given in Fig. 7. Failure occurred without visible local necking of the material and at high strains. The recorded failure stresses and strains are given in

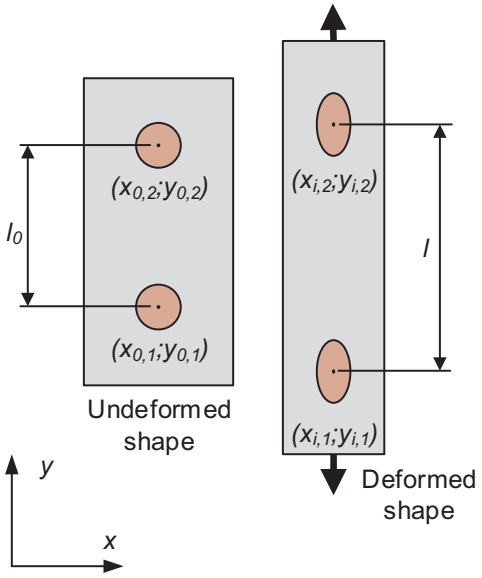

Fig. 6. Video-extensometry.

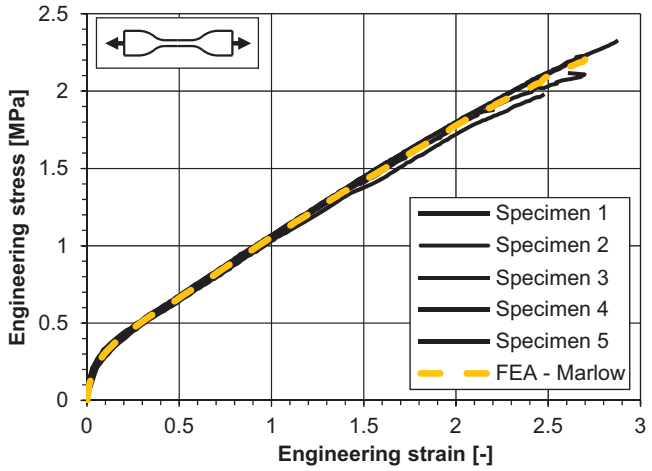

Fig. 7. Results of the uniaxial tension test.

Table 1
Results of the uniaxial tensile test.

Specimen	Isochoric stress [MPa]	True strain [-]
Specimen 1	8.980	1.353
Specimen 2	8.208	1.304
Specimen 3	8.288	1.311
Specimen 4	7.788	1.307
Specimen 5	6.848	1.244
Average	8.023	1.304

Table 1. Failure was observed in the area of parallel edges as shown in Fig. 8. The location of the rupture does not seem to be influenced by the presence of the red silicone marks for video-extensometry.

4.4. Numerical simulation

For the numerical simulation, the commercial Finite Element software code ABAQUS® [28] was used. The silicone was modelled assuming a hyperelastic and incompressible material law. Due to the local measurement of the strains, only one eight of the specimen was modelled due to symmetries in all three directions, as shown in Fig. 9. 20

Fig. 8. Failed tensile test specimens.

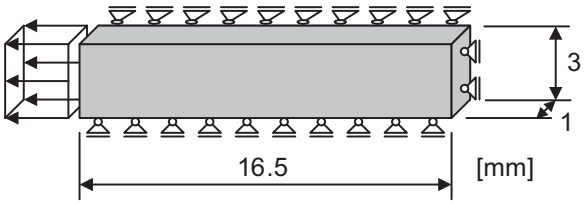

Fig. 9. Boundary conditions of the numerical simulation of the uniaxial tension test.

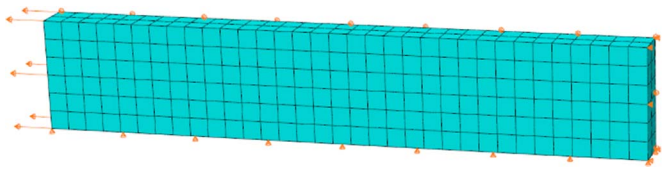

Fig. 10. Numerical model of the uniaxial tension test.

node fully integrated hybrid solid elements (C3D20H) were used to discretise the sealant. The chosen mesh is displayed in Fig. 10. The Marlow hyperelastic material law was used for the sealant. Compared to classical functional expressions for the strain energy potential, like Neo-Hooke, Mooney-Rivlin and Yeoh, the Marlow model is the only one, which is able to reproduce the initial highly non-linear part of the stress-strain curve [12]. High order functional expressions for the strain energy density have not been considered, since the material response was only characterised with a single set of test data (uniaxial tension). The results of the numerical simulation are given in Fig. 7. Very good agreement with the experimental test data is found, since the experimentally obtained stress-strain curve is the basis for the material law's characterisation.

5. Circular shear test

5.1. Specimen

After the determination of the failure in uniaxial tension, simple shear is considered. For the load bearing behaviour in shear, H-shaped specimens as detailed in ETAG 002 [5] are generally used for silicone sealants. As aforementioned, a shortcoming of this specimen is that a stress singularity at the corner edge inhibits a reliable assessment of the stresses, when evaluating the stress state in a Finite Element Analysis. Apart from the numerical phenomena, the corner edge is actually a highly stressed region, which influences the results, when considering failure of the bulk material. In order to eliminate the influence of the corner edge region, the H-shaped specimen was change to a circular specimen, as shown in Fig. 11, and loaded in torsion to obtain a shear stress state within the adhesive.

The alternative approach to avoid the stress concentration in the

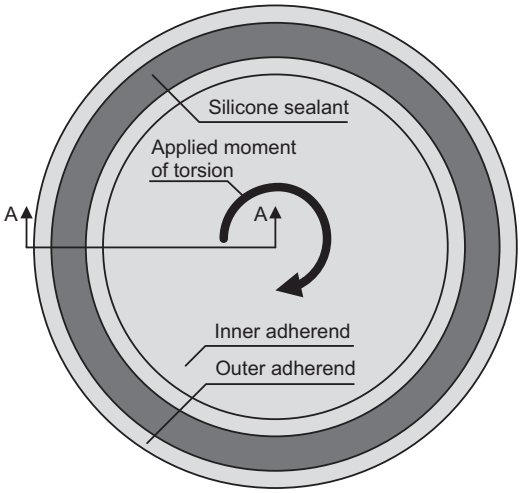

Fig. 11. Circular shear test specimen.

corner edge, as proposed in [29], which consists in inserting fillets at the corner edges, was not used for the present tests, as a fillet does not eliminate the singularity at the corner edge, but only reduces its ”strength” [30].

Tubular lap joints subjected to torsion have already been investigated in [31], where analytical solutions for the stress distribution along the bite direction of the adhesive layer were given. Considering a very soft adhesive compared to the adherend, a constant stress distribution in bite direction is obtained. In [31], the stresses are assumed to be constant along the adhesive layer thickness.

The cross-section of the specimen is shown in Fig. 12. The specimen is composed of two tubes, the one placed into the other and bonded together with silicone. The outer adherend has a diameter of 170 mm, see Fig. 12. A plastic setting block is placed inside the outer adherend to position the inner adherend and to carry its dead load. The circular silicone bead has a thickness of 8 mm and a bite of 16 mm. A ring out of Polytetrafluoroethylene (PTFE) was placed between the silicone joint and setting block in order to avoid adherence on three sides.

The steel parts, the setting block and the PTFE spacer were developed at the University of Luxembourg and produced in-house in the metalworking shop. Prior to the pouring of the silicone sealant, the specimens were carefully cleaned using an appropriate solvent (Dow Corning® R40) and prepared to the sealing using the Dow Corning® 1200 OS primer, as recommended by the manufacturer. The Dow Corning® 993 structural silicone sealant was poured at the Hunsrücker Glasveredelung Wagener, a façade manufacturer in Kirchberg, Germany, using a professional mixing device. After the sealing, the

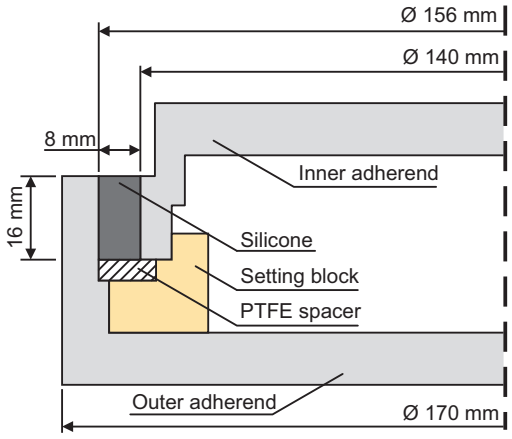

Fig. 12. Section A-A of the circular shear test specimen.

Fig. 13. Test setup for the circular shear test.

specimens have been stored at controlled conditions at the manufacturing facility for two weeks. A number of five specimens has been produced and tested.

5.2. Test setup and measurement equipment

The test series has been performed at the laboratory of the Institute of Steel Construction and Materials Mechanics at TU Darmstadt using a tension-torsion testing machine in an air conditioned environment with 20°C and 50% relative humidity. To apply a torsional moment on the specimen, an adapter was manufactured. It consisted of a disk, welded on a stainless-steel cylinder. The disk was fixed on the top surface of the specimen with screws and the cylinder was inserted into the clamps of the testing machine and also fixed with screws. A second adapter was used for the bottom side of the specimen. The specimen, installed in the testing machine, is shown in Fig. 13 with a detailed view of the specimen given in Fig. 14.

The torsional moment was measured using the load cell of the Schenck testing device. In addition, two displacement transducers were used to measure indirectly the angle of rotation and the relative displacement of the adherends in axial direction. For the measurement of

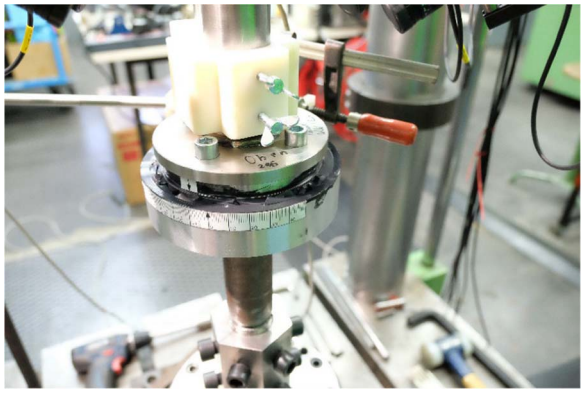

Fig. 14. Installation of the specimen inside the torsion testing machine.

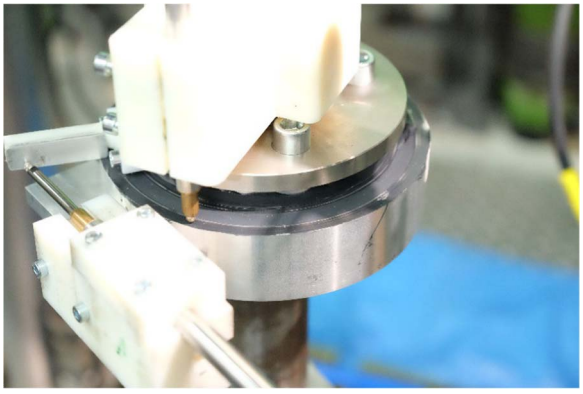

Fig. 15. Displacement transducers used to measure the angle of torsion and the relative axial deformation between the substrates.

the angle of rotation, a displacement transducer was fixed at the outer adherend, as displayed in Fig. 15. A plate was attached on the upper adherend, against which the displacement transducer could measure. The angle was determined considering the non-linear trigonometrical relationships knowing the distance between the centre of the specimen and the axis of the displacement transducer.

The loading rate was determined following the principle of constant energy input. A loading rate of 1.5°/min was used. Axial forces have been set to zero.

5.3. Test results

The torsional moment versus torsional angle diagrams are given in Fig. 16. The exact definition of the failure point is difficult. If one failure criterion is the "occurrence of clearly visible cracks", then it becomes clear that the maximum recorded force might not be an adequate property to quantify the failure initiation load, see specimen 2 in Fig. 16. For this specimen, the first visible cracks appeared at a torsional moment of 850 Nm. This question has already been discussed in [15], where a number of simple shear tests with different geometries have been tested and the tests have been recorded with a video camera. For these tests, a correlation between the appearance of a significant crack and a change of slope or an offset in the force-deformation diagram was found. This result was used to evaluate the specimens of the circular shear test.

The results of the failure load and the failure displacement are given in Table 2. Fig. 17 shows a specimen with the typical saw tooth-shaped cohesive failure pattern of the adhesive layer. A detail picture of this pattern is given in Fig. 18. It is supposed that the saw tooth shaped

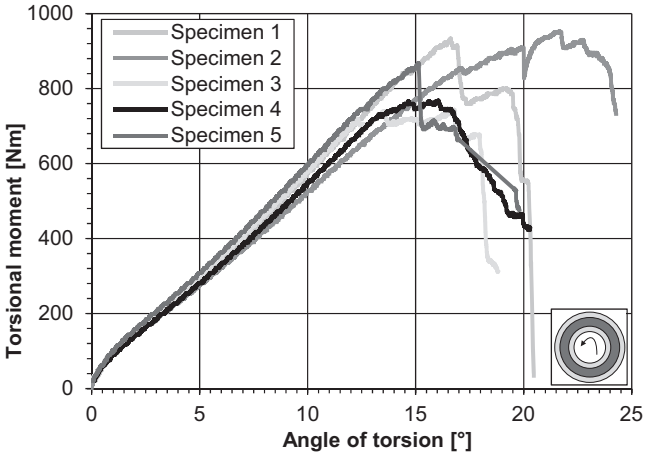

Fig. 16. Results of the circular shear test.

Table 2
Results of the circular shear test.

Specimen	Angle of torsion [°]	Moment of torsion [Nm]
Specimen 1	14.40	840.72
Specimen 2	17.09	854.53
Specimen 3	12.28	717.38
Specimen 4	12.99	717.43
Specimen 5	12.44	745.09
Average	13.8	775.0
Standard dev.	2.0	67.4

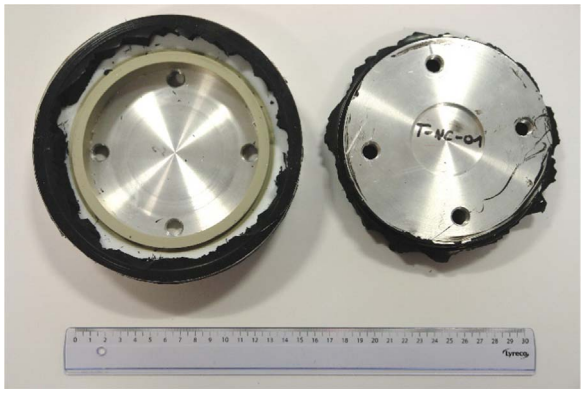

Fig. 17. Failed specimen.

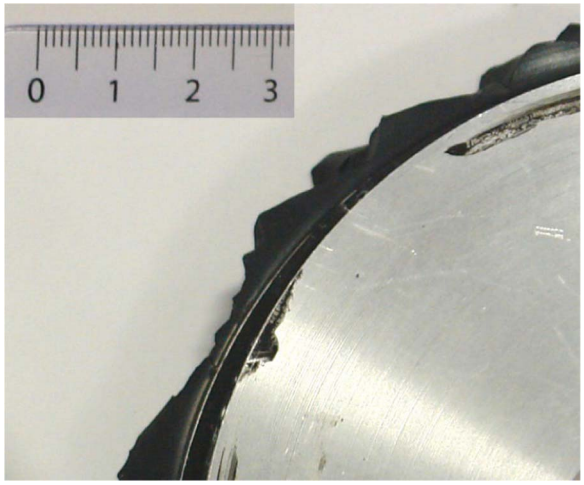

Fig. 18. Detail of Fig. 17.

failure pattern is due to the presence of fillers, which have a much higher strength and stiffness as the soft polymer matrix, thus leading to a change of direction of the crack.

Regarding the external displacement transducer, which monitored the axial displacement, a maximum axial separation distance of 0.5 mm was found with an average value of 0.22 mm for the 5 specimens. A maximum axial compression displacement of 0.1 mm was found with an average of 0.02 mm for the 5 specimens. Due to the small values, these displacements were neglected for the numerical analysis, which is discussed later.

5.4. Numerical simulation

The circular shear tests have been numerically reproduced using the commercial Finite Element software code ABAQUS® [28]. The Marlow hyperelastic material law was chosen to describe the material behaviour of the silicone sealant with the assumption of incompressible

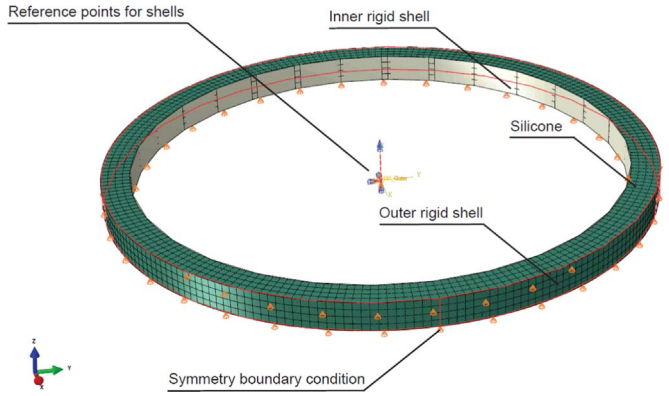

Fig. 19. Boundary conditions for the numerical simulation of the circular shear test.

material behaviour. Symmetry in bite direction was used and the adherends were considered as analytically rigid shells, as they are much stiffer than the soft sealant. The boundary conditions are visualised in Fig. 19.

Quadratic, fully integrated hybrid solid elements (C3D20H) have been used to discretise the sealant. A tie constraint was defined between the rigid shells and the solid elements. The inner rigid shell was fully fixed at its reference point and a rotation was applied on the reference point of the outer rigid shell. A preliminary mesh study showed that the results for the stresses have a convergent behaviour for a reasonably refined mesh with 2 mm element size.

The results of the numerical simulation regarding the global stiffness of the considered connection are given in Fig. 20 in comparison with the average experimental curve. A very good agreement is found between the two curves. The failure process is not covered by the simulation, but will be discussed in Section 7. A plot of the Finite Element software used, displaying the first principal stress acting in the silicone sealant at the failure load, is shown in Fig. 21. The maximum stress is obtained at the inner adherend. The stresses are homogeneous in bite direction. The same result applies for the strains.

6. Compression test

6.1. Methodology

Small silicone cylinders have been loaded in uniaxial compression in order to identify the failure initiation. A number of preliminary test series have been conducted. These tests showed that unlike for the tensile and circular shear tests, a permanent inelastic deformation occurs prior to visible crack initiation. The load level, at which the

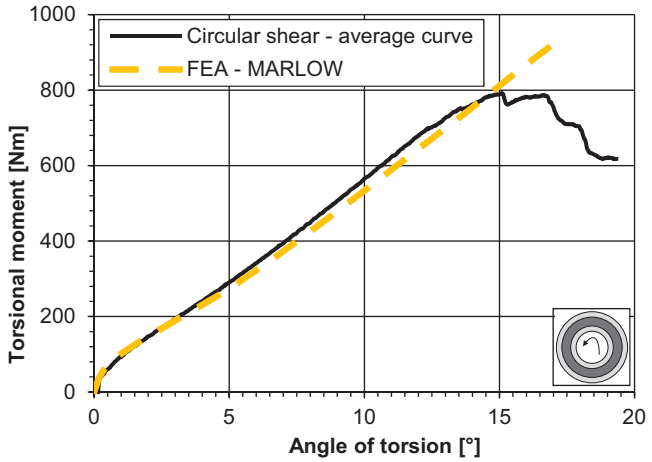

Fig. 20. Comparison of the test results with the Finite Element Analysis.

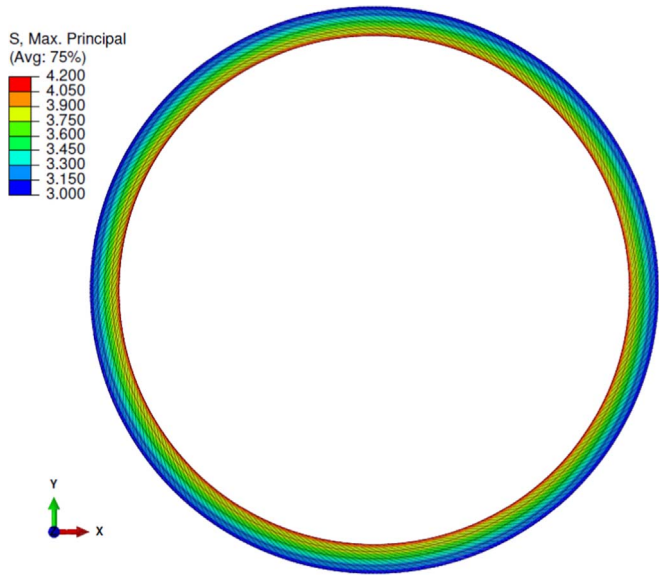

Fig. 21. Plot of the first principal stress, in MPa, calculated using a Finite Element Analysis.

amount of permanent deformation significantly increases, is referred to as the failure initiation point. It is assumed that this permanent deformation can be associated to the material's damage inception.

6.2. Specimen

The geometry of the specimen is a cylinder with a diameter of 12 mm and a height of 12 mm. The specimen is shown in Fig. 22. A mould made of polytetrafluoroethylene (PTFE) was used to produce the specimens. The Dow Corning® 993 structural silicone sealant has been poured under controlled conditions at a façade manufacturer, the Hunsrücker Glasveredelung Wagner, in Kirchberg, Germany, using a professional mixing plant. The manufacturing process is the same as described in [2]. After the pouring of the silicone, the specimens have been stored for one week at ambient conditions at the manufacturer's workshop.

6.3. Test setup and measurement equipment

For the test, a 10 kN hydraulic press was used. The specimen was inserted between two 50 mm thick polished steel plates. No lubricant was used, since a set of preliminary tests showed, that friction could not be avoided even when the plates were greased. In addition, the use of lubricant is an additional parameter of influence, which affects the measured force-deformation behaviour.

The relative displacement between the polished plates was measured using two displacement transducers. The forces have been recorded with two load cells. The tests have been conducted at ambient conditions. The test setup is shown in Fig. 23.

The compression tests have been carried out in displacement control

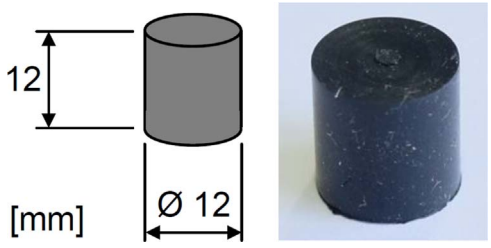

Fig. 22. Test specimen of the compression test.

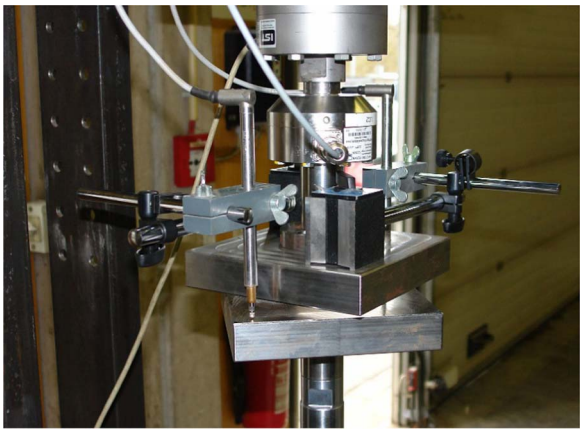

Fig. 23. Compression test setup at University of Luxembourg.

Fig. 24. Thickness gauge to determine the remaining thickness of the specimens.

under a loading rate of 1.44 mm/min in order to have the same engineering strain rate in vertical direction, as recorded in the uniaxial tensile test series. Each specimen has been measured before being tested. The specimen have been loaded in steps of 10% engineering compression strain. After each load step, the specimens were unloaded and their dimensions measured immediately afterwards with the thickness gauge shown in Fig. 24. Additionally, three specimens have been loaded to 50%, 60% and 70% engineering compression strain in one step. The dimensions of these specimens have been recorded as well before and after the test.

6.4. Test results

The test results in terms of engineering stress-strain curves are plotted in Fig. 25 for a specimen loaded in steps of 10% engineering compression strain and for a specimen loaded up to 90% engineering compression strain in one step (referred to as ”90% compression strain”). The repeatedly loaded specimen exhibits the Mullins effect, which was discussed in Section 3. When the specimen is extended

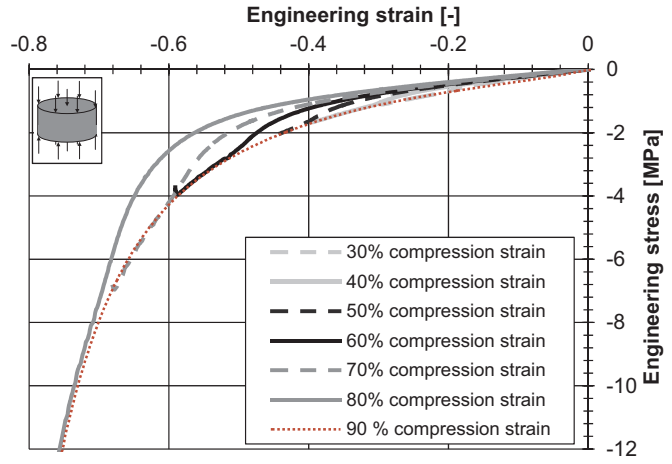

Fig. 25. Engineering stress strain curve.

beyond the maximum previously applied stretch, the stress-strain curve follows the initial stiffness.

After each applied compression strain, the specimens have been unloaded and their dimensions measured using the previously described tools. After each step, the remaining engineering compression strain has been determined. It is defined as follows:

$$\varepsilon_{R,i} = \Delta h/h_0 = (h_i - h_0)/h_0 \tag{8}$$

In equation 8, $\varepsilon_{R,i}$ is the remaining engineering compression strain after step i, h_0 the initial height of the specimen and h_i the height of the specimen after step i. Fig. 26 shows the remaining compression strain plotted against the applied compression strain. A remaining deformation can be observed even for small applied strains. The shape of the curves shown is linear up to an applied engineering compression strain of 60%. A linear regression of the curves between 0 and 60% gives a very good coefficient of determination of more than 98%. In [32], the Mullins effect has been investigated on rubber specimens loaded in tension. A residual strain was observed for repeatedly loaded tensile specimens and a linear relationship was found between the applied tensile stretch and the measured residual strain. Taking into consideration these findings, the observed linear distribution of the remaining strain is assigned to the Mullins effect. Starting from 60% applied compression strain, the remaining deformation strongly increases and this value is taken as a threshold for a significant damage inception, even if no failure in terms of a visible crack was observed.

Fig. 27 shows a specimen during the test between the two polished steel plates and the specimen after unloading. During the tests, the effect of friction is clearly visible. Preliminary tests have shown, that the

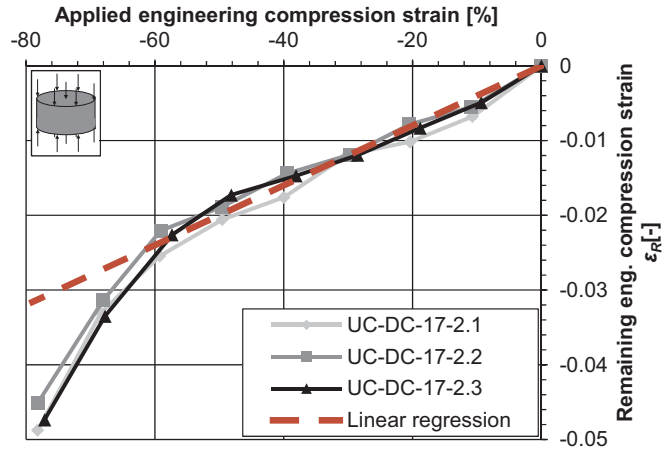

Fig. 26. Remaining compression strain.

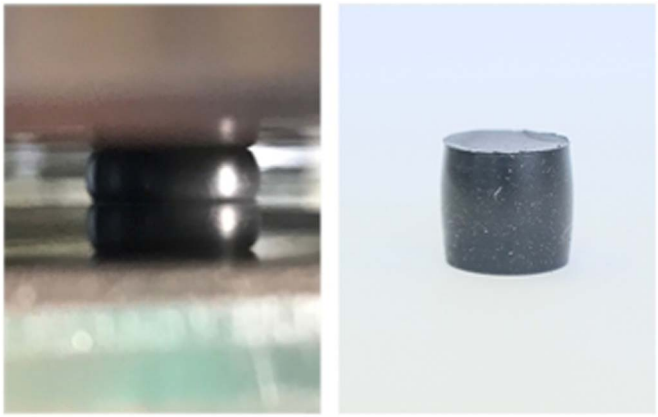

Fig. 27. Test specimen during (left) and after test (right).

use of a lubricant reduces the constrained lateral displacement, but cannot eliminate it. The unloaded specimen displayed in Fig. 27 has no longer a cylindrical shape, but the shape of a wine barrel with the diameter of the specimen at mid-height being larger than the diameter at the upper and lower surface.

In order to check, if the observed residual strains decline as a consequence of viscoelastic effects, the dimensions of the specimens have been measured once again 6 months after the tests. During these 6 months, the specimens have been stored in ambient conditions. The heights of the specimens prior to the tests, after the tests and after 6 months of storage are given in Fig. 28. Additionally, the maximum applied engineering compression strain is indicated for each specimen. For the specimens loaded up to 70% engineering compression strain, the residual height increased by less than 0.2%. For the specimens loaded beyond 80% engineering compression strain, the residual height increased by 1.3% to 8.5%. The latter value was observed for the specimen loaded to an engineering compression strain of 92%. Although a small recovery of the height was observed, the observation that the remaining strain significantly increases starting from 60% applied engineering compression strain, still holds in a quantitative and qualitative way.

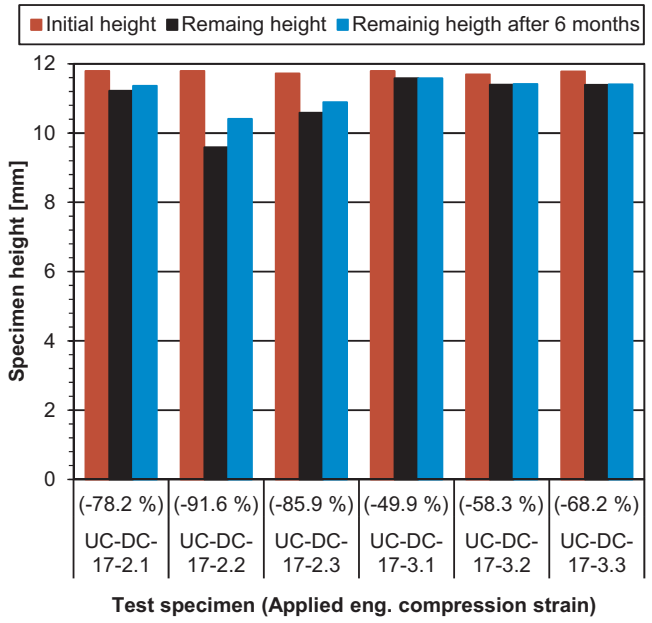

Fig. 28. Heights of the specimens measured before and after the tests, as well as after 6 months of storage.

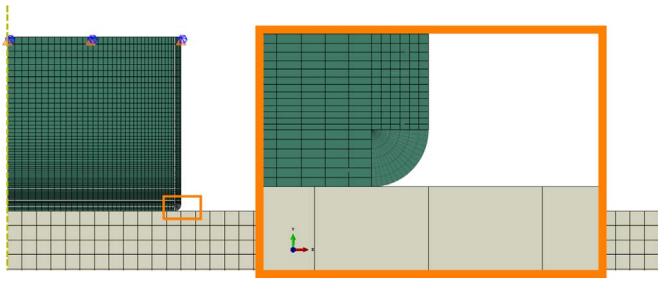

Fig. 29. Finite Element model of the compression test specimen.

6.5. Numerical simulation

The previously described tests have been numerically reproduced using the commercial Finite Element software code ABAQUS®. The Marlow hyperelastic material law with the assumption of incompressible material behaviour was used in the geometrical nonlinear axisymmetric analysis. Quadratic hybrid fully integrated 2D elements (CAX8H) have been used to describe the sealant. The compression plate was modelled as well and the displacements were applied using a reference point and kinematic coupling with the steel plate. Symmetry in vertical direction was used. Fig. 29 shows the numerical model and its boundary conditions.

Due to the large deformations and the restrained lateral dilatation at the compression plates due to friction, the vertical surfaces of the silicone come into contact with the horizontal surfaces of the polished steel plates. In order to avoid a highly distorted mesh at the corner edge, a rounding was inserted. A preliminary numerical study showed that the size of the rounding has only minor influence on the global force-deformation behaviour. Furthermore, minor effect was noticed for the maximum values of the first principal stress and the strain magnitude. Roundings of 0.1 to 0.5 mm have been investigated and a rounding with the radius of 0.25 mm was chosen for the subsequent analysis. A preliminary mesh study also showed that the results concerning force-deformation gave convergent results for the selected element size.

A penalty-based friction formulation in tangential direction and a hard contact in normal direction were chosen to describe the interaction between silicone and steel. Values of the friction coefficient μ between 0.1 and 0.3 were investigated. In addition, the two limits frictionless and bonded behaviour were considered as well. In [33], compression tests on small polyurethane cylinders have been numerically modelled assuming a friction coefficient of $\mu = 0.3$. Fig. 30 shows the comparison between the experimentally recorded stress-strain relations and the numerical simulation for different friction coefficients. A

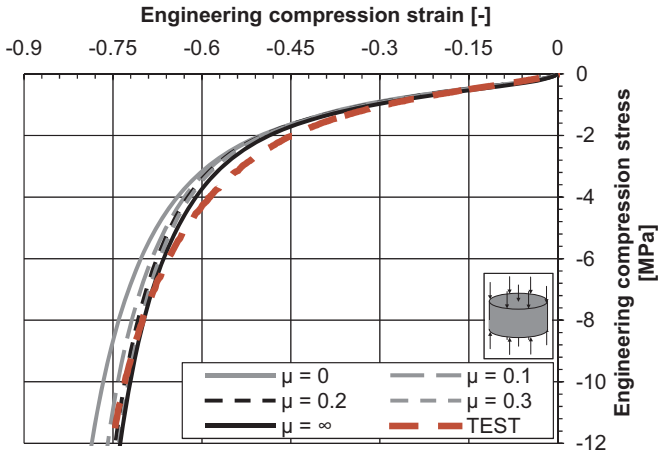

Fig. 30. Results of the Finite Element Analysis for different friction coefficients in comparison with the experimental data.

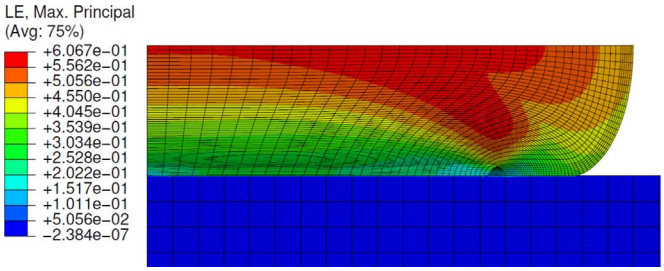

Fig. 31. Plot of the first principal stress, calculated using a Finite Element Analysis.

Table 3
Mesh sensitivity study on stresses and strains at the corresponding deformations at failure.

Test	Number of elements	σ_I [MPa]	ε_M [-]
Tension	51	8.290	1.607
	396	8.290	1.607
	3168	8.290	1.607
Circular shear	466	4.174	1.478
	3714	4.167	1.475
	12528	4.177	1.478
Compression	2103	1.180	1.613
Friction coefficient	3611	1.181	1.612
μ = 0.1	8368	1.181	1.612

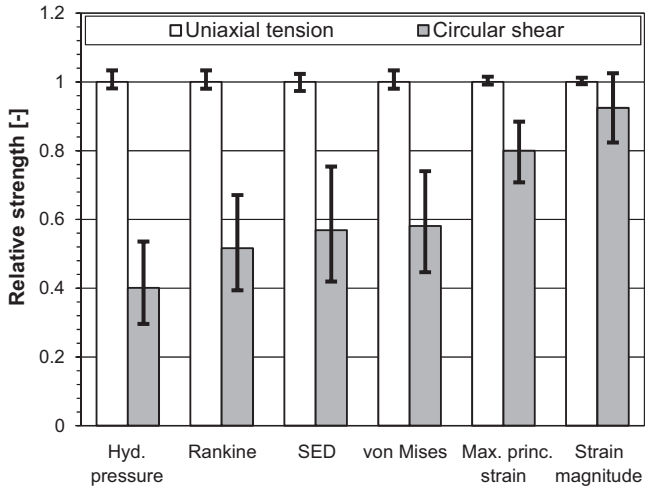

Fig. 32. Comparison of the results regarding different failure criteria with the range of standard deviation - SED is the strain energy density.

good agreement is found.

The distribution of the first principal strain is shown in Fig. 31. As aforementioned, the lateral surface of the silicone specimen came into contact with the horizontal compression plate.

7. Evaluation of the tests regarding existing failure criteria

7.1. Methodology

For the identification of a suitable failure criterion for linear adhesively bonded connections with silicone, two steps were performed. In the first step, the failure criteria, which have been presented in Section 2, were investigated regarding the experimental results obtained in the tensile and circular shear test. For both tests, the stress states at the respective failure loads were determined using a Finite Element Analysis. In the second step, the proposed criterion was validated with the compression test data.

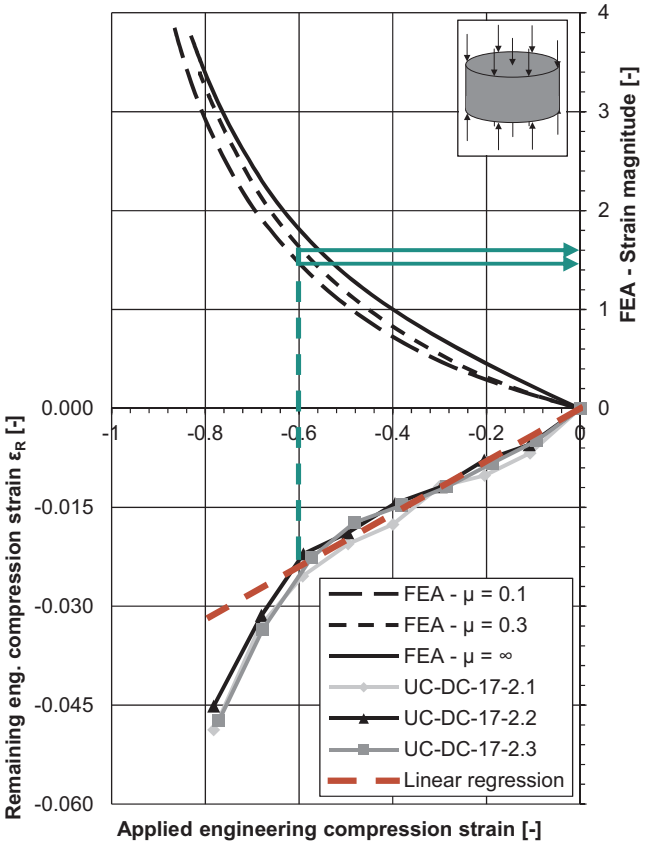

Fig. 33. Remaining engineering compression strain measured in the experimental investigations and results of the Finite Element Analysis for the strain magnitude in the compression test specimen plotted against the applied engineering compression strain.

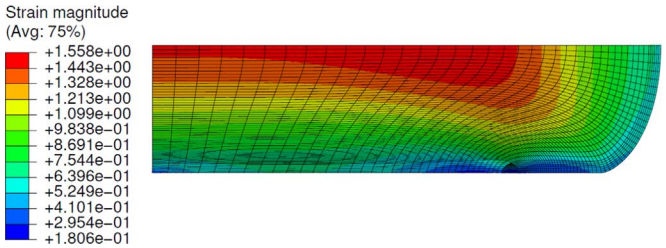

Fig. 34. Plot of the strain magnitude for compression specimen at failure.

7.2. Identification of a failure criterion

For the evaluation of the considered failure criteria, the specimens of the experimental investigations have been numerically reproduced in a non-linear Finite Element Analysis. Details about the model and a comparison with the experimental results regarding the force-deformation behaviour can be found in the previous sections. Convergence in the results of the Finite Element simulations is a fundamental requirement of the assessment of the stresses or strains in the bulk material. Apart from mesh studies on the global force-deformation behaviour, the convergence of the stresses and strains has also been checked for the numerical models of the three tests. Table 3 gives the obtained values for the largest first principal stress σ_I in the test specimens and the strain magnitude ε_M as a function of the number of elements used in each model. Good convergence was obtained for the three models.

In this section, the presented failure criteria are investigated. For each simulation, the deformation at failure was applied on the specimens and the obtained stress and strain states were evaluated regarding the following failure criteria: the hypothesis of Rankine, the hydrostatic

pressure, Von Mises, the maximum principal strain and the strain energy density (SED). In addition, the strain magnitude was determined out of the three principal true strains. For each hypothesis, the stress states obtained for the average failure displacement as well as the standard deviation added and subtracted from the average value, have been analysed.

The results of these simulations are displayed in Fig. 32. For each considered failure criterion, the relative strength is compared between the investigated stress states tension and shear. The relative strength is the ratio of the value (stress, strain or energy) obtained from the numerical analysis of the respective test (tension or shear) at its failure load divided by the corresponding strength value from the uniaxial tension test. The error bars show the result for the standard deviation added or subtracted to the average value at failure.

The values for the strain magnitude at failure are given in Table 3. For the uniaxial tensile test, a value of 1.6 is obtained. Fig. 32 shows that almost the same value for the strain magnitude is obtained at the imposed failure load or displacement for both the tension and shear test. The values of the other considered failure criteria do not coincide between tensile and shear test.

7.3. Validation of the proposed criterion

After the strain magnitude has been identified in this campaign as the best fitting engineering failure criterion, the results of the uniaxial compression tests are used to validate the proposed criterion. The compression tests have been numerically reproduced and the strain magnitude distribution has been determined. Fig. 33 shows the maximum recorded value for the strain magnitude in the Finite Element Analysis and the remaining engineering compression strain measured in the test as a function of the imposed engineering compression strain. For imposed engineering compression strains above 60%, the remaining deformation starts to strongly increase. At this level of imposed compression strain, a value between 1.5 and 1.6 is found for the strain magnitude in the Finite Element simulation of the test specimen. The value 1.6 was calibrated with the uniaxial tensile test results.

The maximum value of the strain magnitude is found in the centre of the specimen, as shown in Fig. 34, where the strain magnitude distribution is plotted for the compression specimen.

8. Conclusion and outlook

Tests on a structural silicone sealant have been performed considering the different fundamental stress states tension, shear and compression. These tests have been numerically reproduced with the commercial Finite Element software code ABAQUS®. The silicone sealant has been described with the Marlow hyperelastic material law. A good agreement between the experimental results and their numerical simulation was found. For the three test series, the stress states at the recorded failure loads or displacements have been considered. From these investigations, a simple engineering failure criterion has been identified for structural silicone sealant. Amongst the considered failure criteria, the values for the strain magnitude determined in a Finite Element Analysis for the tension and shear tests at their respective failure loads are in good agreement. The failure criterion has been validated with the compression test results.

The proposed failure criterion of the strain magnitude is based on some fundamental assumptions: Apart from the incompressible hyperelastic material law used in the numerical simulation, only quasi-static loadings and the initial stiffness were considered. Since only basic stress states have been investigated, the proposed failure criterion is only valid for simple geometries, like linear silicone beads. In a next step, additional load schemes, like biaxial tests in form of bulge tests, as done in [34], considering different aspect ratios, or pure shear tests, should be performed to confirm the results concerning the strain magnitude and thus allow for the assessment of more complex geometries.

The fundamental tests to calibrate and validate the proposed failure criterion for simple geometries have been selected with regard to avoid stress singularities and notches. Therefore, the stresses and strains obtained from the numerical analysis are independent of the size of the chosen Finite Elements. The assessment of stresses and strains in vicinity of a stress singularity is subject of a PhD research project at University of Luxembourg in collaboration with TU Darmstadt [17].

Acknowledgements

The authors would like to acknowledge Dr. Thomas Beier and Tobias Brehm from the Institute of Steel Construction and Materials Mechanics, Technische Universität Darmstadt, Germany, for the conduction of the circular shear tests, the Hunsrücker Glasveredelung Wagener in Kirchberg, Germany, for the pouring of the silicone and the Dow Corning company for their continuous support.

References

[1] Tibolt M, Odenbreit C. The stress peak at the borehole of point-fitted IGU with undercut anchors. J Facade Des Eng 2014;2(1-2):33–66. http://dx.doi.org/10.3233/FDE-130011.
[2] Dias V, Odenbreit C, Hechler O, Scholzen F, Zineb TB. Development of a constitutive hyperelastic material law for numerical simulations of adhesive steel-glass connections using structural silicone. Int J Adhes Adhes 2014;48:194–209. http://dx.doi.org/10.1016/j.ijadhadh.2013.09.043.
[3] de Buyl F. Silicone sealants and structural adhesives. Int J Adhes Adhes 2001;21(5):411–22. http://dx.doi.org/10.1016/ S0143-7496(01)00018-5.
[4] Richter C, Abeln B, Geßler A, Feldmann M. Structural steel-glass facade panels with multi-side bonding – Nonlinear stress-strain behaviour under complex loading situations. Int J Adhes Adhes 2014;55:18–28. http://dx.doi.org/10.1016/j.ijadhadh.2014.07.004.
[5] ETAG 002., Guideline for European Technical Approval for Structural Sealant Glazing Kits, European Organisation for Technical Approvals; 2012.
[6] Descamps P, Iker J, Wolf AT. Effects of anodized aluminium surface parameters on the long-term adhesion of silicone structural glazing sealants. Constr Build Mater 1996;10(7):527–38. http://dx.doi.org/10.1016/0950-0618(96)00008-6.
[7] Drass M, Schneider J, On the mechanical behavior of transparent structural silicone adhesive - TSSA, In: Zingoni A. (Ed.), Insights and Innovations in Structural Engineering, Mechanics and Computation: SEMC 2016 - Sixth International Conference on Structural Engineering, Mechanics and Computation, Elsevier B.V., 2016. doi:10.1201/9781315641645-74.
[8] Dow Corning Corporation., Case study: Forum Hochhaus Frankfurt am Main, Germany, Dow Corning Corporation, form number 62-1298C-01; 2010.
[9] Gutowski VW, Russell L, Cerra A. New tests for adhesion of silicone sealants. Constr Build Mater 1993;7(1):19–25. http://dx.doi.org/10.1016/0950-0618(93)90021-4.
[10] Rey T, Chagnon G, Cam J-BL, Favier D. Influence of the temperature on the mechanical behaviour of filled and unfilled silicone rubbers. Polym Test 2013;32(3):492–501. http://dx.doi.org/10.1016/j.polymertesting.2013.01.008.
[11] ASTM C1401. Standard guide for structural sealant glazing. ASTM International; 2002.
[12] Staudt Y, Schneider J, Odenbreit C. Investigation of the material behaviour of bonded connection with silicone, In: Schneider J, Weller B. (Eds.), Engineered Transparency international conference at glasstec, Düsseldorf, Germany; 2014.
[13] Scherer T. Werkstoffspezifisches Spannungs-Dehnungs-Verhalten und Grenzen der Beanspruchbarkeit elastischer Klebungen [Ph.D.-thesis]. Technische Universität Kaiserslautern; 2014.
[14] Weißgraeber P, Becker W. Finite fracture mechanics model for mixed mode fracture in adhesive joints. Int J Adhes Adhes 2013;50:2383–94. http://dx.doi.org/10.1016/j.ijsolstr.2013.03.012.
[15] Staudt Y, Odenbreit C, Schneider J. Investigation of bonded connections with silicone under shear loading, In: Bos F, Louter C, Belis J. (Eds.), Challenging Glass 5 - Conference on Architectural and Structural Applications of Glass, 2016.
[16] Dow Corning Corporation., Dow Corning 993 Structural Glazing Sealant - Product sheet, Dow Corning Corporation, ref. no. 62-0918H-01; 2001.
[17] Staudt Y. Proposal of a failure criterion of adhesively bonded connections with silicone [Ph.D. thesis]. University of Luxembourg / Technische Universität Darmstadt; 2017. [not yet published].
[18] Naït-Abdelaziz M, Zaïri F, Qu Z, Hamdi A, Aït-Hocine N. J integral as a fracture criterion of rubber-like materials using the intrinsic defect concept. Mech Mater 2012;53:80–90. http://dx.doi.org/10.1016/j.mechmat.2012.05.001.
[19] Gross D, Seelig T. Fracture mechanics: with an introduction to micromechanics 2. Springer; 2011.
[20] Gent AN, Lindley PB. Internal rupture of bonded rubber cylinders in tension. Proc R Soc Lond Ser A Math Phys Sci 1959;249(1257):195–205. http://dx.doi.org/10.1016/10.2307/100509.
[21] Zine A, Benseddiq N, Naït-Abdelaziz M. Rubber fatigue life under multiaxial loading: numerical and experimental investigations. Int J Fatigue 2011;33(10):1360–8. http://dx.doi.org/10.1016/j.ijfatigue.2011.05.005.
[22] Molls M. Experimentelle und numerische Untersuchung ein- und mehrachsig

belasteter Elastomerbuchsen unter besonderer Berücksichtigung des Reihenfolgeeinflusses [PhD-thesis]. Universität Duisburg-Essen; 2013.
[23] Machado G, Chagnon G, Favier D. Analysis of the isotropic models of the Mullins effect based on filled silicone rubber experimental results. Mech Mater 2010;42(9):841–51. http://dx.doi.org/10.1016/j.mechmat.2010.07.001.
[24] Wolf A, Descamps P. Determination of Poisson's Ratio of silicone sealant from ultrasonic and tensile measurements [ASTM STP 1422]. In: Johnson P, editor. Performance of exterior building wallsWest Conshohocken, PA: American Society for Testing and Materials; 2002.
[25] Marlow R. A general first-invariant hyperelastic constitutive model, In: Busfield J, Muhr A.(Eds.), Constitutive models for rubber III In: Proceedings of the third European conference on constitutive models for rubber, London, Swets & Zeitlinger, Lisse, pp. 157–160; 2003.
[26] ASTM D412. Standard test methods for vulcanized rubber and thermoplastic elastomers - tension. ASTM International; 2013.
[27] Franz J. Untersuchungen zur Resttragfähigkeit von gebrochenen Verglasungen: investigation of the residual load-bearing behaviour of fractured glazing. [Ph.D.-thesis]. Technische Universität Darmstadt; 2015. http://dx.doi.org/10.1007/978-3-662-48556-9.
[28] Dassault Systèmes., ABAQUS® 6.14 Documentation; 2014.
[29] Grandcoin J, Boukamel A, Lejeunes S. A micro-mechanically based continuum damage model for fatigue life prediction of filled rubbers. Int J Solids Struct 2014;51(6):1274–86. http://dx.doi.org/10.1016/j.ijsolstr.2013.12.018.
[30] Chen Z, Adams R, Da Silva L. The use of the J-integral vector to analyse adhesive bonds with and without a crack. Int J Adhes Adhes 2011;31:48–55. http://dx.doi.org/10.1016/j.ijadhadh.2010.11.005.
[31] Adams R, Peppiatt N. Stress analysis of adhesive bonded tubular lap joints. J Adhes 1977;9(1):1–18. http://dx.doi.org/10.1080/ 00218467708075095.
[32] Dorfmann A, Ogden R. A pseudo-elastic model for loading, partial unloading and reloading of particle–reinforced rubber. Int J Solids Struct 2003;40(11):2699–714.
[33] Sikora P. Materialcharakterisierung und -modellierung zur Simulation von Klebverbindungen mit Polyurethanklebstoffen [Ph.D.-thesis]. Universität Paderborn; 2014.
[34] Drass M, Schwind G, Schneider J, Kolling S. Adhesive connections in glass structures – part I: experiments and analytics on thin structural silicone. Glass Struct Eng 2017:1–16. http://dx.doi.org/10.1007/s40940-017-0046-5.